Seasonal sea ice prediction based on regional indices

John E. Walsh[1], J. Scott Stewart[2], Florence Fetterer[2]

[1]Alaska Center for Climate Assessment and Policy, University of Alaska, Fairbanks, AK 99709 USA
[2]National Snow and Ice Data Center, University of Colorado, Boulder, CO 80303 USA

Correspondence to: John E. Walsh (jewalsh@alaska.edu)

Abstract. Basic statistical metrics such as autocorrelations and across-region lag correlations of sea ice variations provide benchmarks for the assessments of forecast skill achieved by other methods such as more sophisticated statistical formulations, numerical models, and heuristic approaches. In this study we use observational data to evaluate the contribution of the trend to the skill of persistence-based statistical forecasts of monthly and seasonal ice extent on the pan-Arctic and regional scales. We focus on the Beaufort Sea where the Barnett Severity Index provides a metric of historical variations in ice conditions over the summer shipping season. The variance about the trend line differs little among various methods of detrending (piecewise linear, quadratic, cubic, exponential). Application of the piecewise linear trend calculation indicates an acceleration of the winter and summer trends during the 1990s. Persistence-based statistical forecasts of the Barnett Severity Index as well as September pan-Arctic ice extent show significant statistical skill out to several seasons when the data include the trend. However, this apparent skill largely vanishes when the data are detrended. In only a few regions does September ice extent correlate significantly with antecedent ice anomalies in the same region more than two months earlier. The springtime "predictability barrier" in regional forecasts based on persistence of ice extent anomalies is not reduced by the inclusion of several decades of pre-satellite data. No region shows significant correlation with the detrended September pan-Arctic ice extent at lead times greater than a month or two; the concurrent correlations are strongest with the East Siberian Sea. The Beaufort Sea's ice extent as far back as July explains about 20% of the variance of the Barnett Severity Index, which is primarily a September metric. The Chukchi Sea is the only other region showing a significant association with the Barnett Severity Index, although only at a lead time of a month or two.

1 Introduction

One of the most widely monitored variables in the climate system is Arctic sea ice. By any measure, Arctic sea ice has decreased over the past few decades (Box et al., 2018). September sea ice extent during the past 5-10 years has been approximately 50% of the mean for the 1979-2000 period (AMAP, 2017). The recent decline is unprecedented in the satellite record, in the period of direct observations dating back to 1850 (Walsh et al., 2016), and in paleo reconstructions spanning more than 1400 years (Kinnard *et al*., 2011). The recent reduction of sea ice has been less in winter and spring than in summer and autumn, resulting in a sea ice cover that is largely seasonal (AMAP, 2017). The increasingly seasonal ice cover contrasts with the Arctic Ocean's predominantly multiyear ice pack of the pre-2000 decades. When compared to the reductions of the spatial extent of sea ice, the percentage reductions of ice volume and thickness are even larger. Ice thickness decreased by more than 50% from 1958-1976 to 2003-2008 (Kwok and Rothrock, 2009), and the percentage of the March ice cover made up of thicker multiyear ice (ice that has survived a summer melt season) decreased from 75% in the mid-1980s to 45% in 2011 (Maslanik *et al*., 2011). Laxon et al. (2013) indicate a decrease of 64% in autumn sea ice volume from 2003-08 to 2012. The portion of the Arctic sea ice cover comprised of older thicker ice has decreased from 45% in 1985 to 21% in 2017 (NOAA, 2018).

While the loss of sea ice is generally presented in terms of pan-Arctic metrics, regional trends can be quite different from the pan-Arctic trends. The Bering Sea, for example, showed a positive trend of coverage (fewer open water days) from 1979 through 2012 (Parkinson, 2014), However, the positive trend of Bering Sea ice largely vanishes when the most recent winters (especially 2017-18) are included. By contrast, the Chukchi and Beaufort Seas to the north of the Bering Sea have shown some of the largest decreases of summer ice coverage in the entire Arctic (Onarheim et al., 2018). Another area of strong decrease of ice coverage has been the Barents/Kara Sea region.

The Beaufort Sea serves as an illustrative example of the impacts of trends and variability of sea ice. The number of open water days immediately offshore of the Beaufort coast has been 60-120 in recent years. Parkinson's (2014) Figure 2 shows that the number of open water days increased by 20-30 days per decade over the period 1979-2013. However, as recently as the 1970s, there were summers with little or no open water in this region, as described by Crowley Maritime, one of the major barge operators in the Alaska region:

> "With pipeline construction well underway in 1975, the Crowley summer sealift flotilla to the North Slope faced the worst Arctic ice conditions of the century. In fleet size, it was the largest sealift in the project's history with 47 vessels amassed to carry 154,420 tons of cargo, including 179 modules reaching as tall as nine stories and weighing up to 1,300 tons each. Vessels stood by for nearly two months waiting for the ice to retreat. Finally in late September the ice floe moved back and Crowley's tugs and barges lined up for the slow and arduous haul to Prudhoe Bay. When the ice closed again, it took as many as four tugs to push the barges, one at a time, through the ice".
>
> *— From Crowley Maritime, 50 Years of Service in Alaska (2002)*

As will be shown, the contrast between present-day ice conditions and the Crowley experience of the 1970s is largely a manifestation of the trend of Beaufort Sea ice cover. However, sea ice also exhibits large year-to-year variability, which has been superimposed on the recent trend towards less sea ice in the Arctic. This variability challenges users of coastal waters in various sectors and lies at the heart of the sea ice prediction problem. While the climatological seasonal cycle and even observed trends provide an initial expectation for the sea ice conditions that will be present in a particular region at a particular time of year, the departures from the climatological mean, whether or not the mean is adjusted for a trend, is affected by the atmospheric forcing (winds, air temperatures, radiative fluxes) and oceanic forcing (currents, water temperatures) of the particular year in addition to antecedent ice conditions themselves. These departures have a large component of internal variability and hence are difficult to predict over monthly and seasonal timescales (Serreze et al., 2016), raising questions about the extent to which sea ice variations may be predictable. Even ice-ocean models initialized to current sea ice and ocean conditions require atmospheric forcing in order to predict future ocean states. Moreover, fully coupled models, which determine both the atmospheric and ocean/ice conditions prognostically, are now used increasing often for seasonal sea ice predictions. Ensembles of coupled simulations are generally run because of the chaotic nature of the climate system. These models can be run for much longer time periods than the observational sea ice record, so they can provide statistics of sea ice persistence (autocorrelations) subject to the "perfect model" assumption. Examples of studies employing the "perfect model" approach are Holland et al. (2011) Blanchard-Wrigglesworth et al. (2011), Day

et al. (2014), Bushuk et al. (2017) and Bushuk et al. (2018). In these model simulations, autocorrelation of sea ice anomalies tends to be greater in the model results than in observational data (e.g., Blanchard-Wrigglesworth et al., 2011, their Fig. 2; Day et al., 2014, their Fig. 1).

The skill of persistence-based statistical forecasts of sea ice variations beyond the mean seasonal cycle and ongoing trends is the main focus of this paper. While various prior studies (cf. Section 2) have utilized broader approaches to evaluating sea ice predictability and the skill of forecasts, the present study is limited specifically to statistical predictions of regional (and pan-Arctic) September sea ice based on auto-correlation (anomaly persistence, often referred to as "memory") and lagged cross-correlations between with other sea ice coverage quantities. Other approaches to sea ice predictability include the use of models, which can be initialized to obtain deterministic forecasts verifiable with observations or which can be run for long periods in a coupled mode to assess predictability of sea ice within the "model's world" (irrespective of observations). We also do not use atmospheric or oceanic predictors in our evaluation of persistence-based predictability. Atmospheric predictors in the form of known teleconnection patterns have been used by Drobot (2003) and Lindsay et al. (2008), while Bushuk et al. (2017) have shown that ocean temperature initialization contributes to skill of seasonal forecasts of sea ice in the North Atlantic subarctic seas. A review of the various approaches to sea ice prediction and sources of predictability has been provided by Guemas et al. (2016).

The present paper extends the temporal window of Drobot's (2003) study of the predictability of Beaufort-Chukchi sea ice. Drobot used data from 1979-2000 to assess predictability of a measure of Beaufort Sea summer ice severity (Section 3 below) based on antecedent sea ice conditions as well as several atmospheric indices. While the present study will not include the type of multiple-predictor evaluation carried out by Drobot, it will provide a more comprehensive and updated assessment of sea ice anomaly persistence in a predictive context. Drobot (2003) found that, in predictions based on indicators from the previous seasons, the limited sample of years used in developing the statistical models raises questions about broader applicability. In this regard, Drobot (2003, p. 1161) states "…if the Arctic climate changes, the methods described here will need to be altered". In fact, the Arctic climate and, in particular, its sea ice regime, have changed with the unprecedented retreat of sea ice in the post-2000 period. The impact of the trend on statistical predictability is a focus of the present paper. Another relevant study is that of Blanchard-Wrigglesworth et al. (2011), who found evidence that

persistence of ocean temperature anomalies across seasons has a detectable impact on sea ice variations, implying some predictability over seasonal timescales.

In the present paper, we use the autocorrelation statistic to quantify the skill of persistence as a control forecast of pan-Arctic and regional sea ice extent. In addition to utilizing the more conventional metric of ice extent in regional and pan-Arctic domains, we include a regional sea ice index developed in the 1970s to capture interannual variations of marine access in the Beaufort Sea. A primary focus of the evaluation is the method of detrending the data, as various alternative methods have not been fully explored in the literature. We show that the piecewise linear method generally results in the smallest residual variance about the trend line, and we then perform an across-region synthesis of information on the break-points of the two-piece linear trend lines in different seasons. Our period of analysis extends back to 1953, which results in a considerably larger sample of years than the more commonly used satellite period (1979 onward). Finally, we examine lagged cross-correlations to determine whether pan-Arctic ice extent or Beaufort Sea summer ice conditions are foreshadowed in a statistical sense by antecedent ice conditions in particular subregions of the Arctic.

More generally, the results presented here can serve to provide a baseline for distinguishing contributions to seasonal sea ice forecast skill arising from climatological sea ice coverage, sea ice persistence, and sea ice trend. This baseline can, in turn, serve as benchmarks for measuring improvements achieved by more sophisticated prediction approaches such as dynamical models, analog systems, neural networks and other more comprehensive statistical methods. The Sea Ice Outlook, coordinated by the Sea Ice Prediction Network now in its Phase 2 (https://www.arcus.org/sipn/sea-ice-outlook, accessed 27 Dec 2018)), provides an annual compilation of seasonal sea ice forecasts, which are grouped into three categories: physical/dynamical models, statistical methods, and heuristic approaches. While the methodology used in this paper falls into the statistical category, the distinctions between (a) pan-Arctic and regional skill and (b) trend-derived and interannual forecast skill are relevant to all three approaches to sea ice prediction.

2. Previous work

The baseline for persistence-based predictions have been established in previous studies (e.g., Blanchard-Wrigglesworth et al., 2011; Day et al., 2014; Bushuk et al., 2017, 2018). These studies have generally focussed on the post-1979 period of satellite data, while the present study a longer record length (back to 1953 rather than 1979). The main intent of the paper is to show how detrending is a key step in the depiction of persistence-based statistical predictions. We illustrate the effect of detrending for both pan-Arctic ice extent and regional metrics in order to show that predictive applications on both scales must address detrrending in a rigorous way, and that there are various alternatives for detrending. While these alternative detrending strategies are known, the relative effectiveness of the various alternatives has not been addressed in previous studies. Goldstein et al. (2016; 2018) come closest by comparing representations based on linear trends and discontinuities in the mean. An additional novel outcome of the present study is the synthesis of break-point information.

The extension back to 1953 is especially noteworthy because of the recent reduction of Arctic sea ice coverage has occurred almost entirely in the post-1978 period of satellite coverage. On both pan-Arctic and regional scales, ice extent was relatively stable during the 1950s, 1960s and 1970s, although interannual variations were still a prominent feature of the time series (Walsh et al., 2016). While Drobot (2003) and Lindsay et al. (2008) made use of sea ice data extending back to the 1950s, there has been no systematic comparison of sea ice anomaly persistence during the satellite era with anomaly persistence over longer time periods.

3. Metrics of sea ice coverage

Historical variations of sea ice are documented using various metrics, including sea ice extent, ice-covered area, and thickness. Sea ice extent is the total area within the ice edge, which is typically taken to be the 15% contour of sea ice concentration. Ice extent is readily obtainable from satellite measurements, as is the actual ice-covered area if the open water within the ice edge is accurately depicted. Surface-based observations from ships or coastal locations typically capture only the ice edge and are therefore useful primarily in the mapping of ice extent. While digitized records of ice extent exist back to the 1800s, there are no such historical products for ice thickness. *In situ* measurements of ice thickness are sparse in space and time, as are submarine sonar measurements, which are not only sparse but often remain unavailable. Satellite-derived estimates of ice thickness are subject to considerable uncertainty and have only

recently come into use (e.g., CryoSat), while dynamic-thermodynamic model-based reconstructions of historical sea ice thickness variations have only recently been attempted (Schweiger et al., 2018).

To explore the statistical skill that may be inherent in the spatial distribution of sea ice, we compute ice extent using the gridded Arctic-wide sea ice concentration product known as "Gridded Monthly Sea Ice Extent and Concentration, 1850 Onward (Walsh et al., 2015), referred to in the National Snow and Ice Data Center (NSIDC) catalog as G10010. This dataset is based on observations from approximately 15 historical sources between 1850 and 1978: the earliest are whaling records, and the most complete, in terms of coverage, are the Arctic-wide analyses that the U.S. National Ice Center (NIC) began in the early 1970s. Beginning in 1979, sea ice concentrations from passive microwave data are used exclusively in G10010. Ice concentration fields on the 15th of each month are taken from the *NOAA/NSIDC Climate Data Record of Passive Microwave Sea Ice Concentration, Version 2 (Meier et al., 2013).*

Prior to the 1950s, most observations were from near or just within the ice edge. If only the ice edge position was known, a gradient of ice concentration within the edge was imposed in order to integrate the observations into G10010. The gradient was based on a climatology constructed from the passive microwave data. Spatial and temporal gaps in observations were filled using an analog technique that is described in the data product documentation. Each month's sea ice concentration field in G10010 is an estimate of conditions at one time in the month, nominally the 15th day of the month (or as close to the 15th as data were available). The fields are at quarter-degree resolution. From these fields one can derive monthly sea ice extent values. Sea ice extent is computed as the area, in sq km, covered by all cells that contain ice in any concentration greater than 15%. Sea ice extent is always greater than or equal to the actual ice-covered area, which excludes the area of open water within the main ice pack.

Various studies (e.g. Partington et al., 2003; Agnew and Howell 2002) have shown that passive microwave-derived sea ice data tend to underestimate ice concentration when compared with operational analyses. The *Climate Data Record of Passive Microwave Sea Ice Concentration* is a blend of output from two algorithms that results in higher ice concentrations overall for a better match with the operational analyses that predate the satellite record. Even so, one might expect to see a discontinuity in the G10010 time series of ice extent when the passive microwave record starts in 1979, but this is not evident (see Fig. 10 in Walsh et al.,

2016). While G10010 gives a record of ice extent that has realistic variability back to 1850, it is difficult to assign an uncertainty to the concentration fields and ice extent values derived from them. Ice extent will be more accurate than actual ice-covered area because there are many more observations of the ice edge than of the concentrations within interior pack. For this reason, we base our analysis on ice extent. It should be noted, however, that persistence time-scales of pan-Arctic sea ice area have been shown in previous studies (e.g., Blanchard-Wrigglesworth et al., 2011) to be longer than those of pan-Arctic sea ice extent because high-frequency forcing can change ice extent more than it changes ice area (i.e., by converging or diverging ice floes in the absence of ridging or melt).

G10010 was used to compute the time series of monthly sea ice extent for the pan-Arctic domain and various Arctic subregions in which sea ice is at least a seasonal feature. The regionalization adopted here follows that of the MASIE (Multisensor Analyzed Sea Ice Extent) product available from the National Snow and Ice Data Center (http://nsidc.org/data/masie/browse_regions, accessed 27 Dec 2018). MASIE (NIC and NSIDC, 2010) is produced in cooperation with the NIC, and its regions are defined on the basis of NIC operational analyses areas. We use the following MASIE regions: (1) Beaufort Sea, (2) Chukchi Sea, (3) East Siberian Sea, (4) Laptev Sea, (5) Kara Sea, (6) Barents Sea, (7) East Greenland Sea, (8) Baffin Bay/Davis Strait, (9) Canadian Archipelago, (10) Hudson Bay, (11) central Arctic Ocean and (12) Bering Sea. There are several other MASIE regions (Baltic Sea, Yellow Sea, Cook Inlet) that are not used here because they are not geographically connected with the main Arctic sea ice cover. Figure 1 shows the regions.

We also make use of the long ice extent record provided by G10010 to investigate the extent to which the Barnett Severity Index, or BSI, may be statistically predictable from antecedent ice extent. The BSI is directly relevant to offshore navigation applications in the Beaufort Sea. It is a metric of the severity of ice conditions, such as conditions encountered by barges resupplying the North Slope. The BSI is determined once per year, at the end of the summer shipping season, by analysts at the NIC. It is a unit-less linear combination of five parameters: 1) the distance in nautical miles from Point Barrow northward to the ice edge on 15 September, 2) the distance from Point Barrow northward to the 4/8th ice concentration line on 15 September, 3) the number of days the entire sea route from the Bering Strait to Prudhoe Bay is ice-free in a calendar year, 4) the number of days the entire sea route to Prudhoe Bay is less than or equal to 4/8th ice

concentration in a calendar year, and 5) the temporal length of the navigable season, defined as the time period from the initial date the entire sea route is less than 4/8th ice concentration to 1 October (Barnett, 1980). Figure 2 is a time series of the BSI reconstructed from gridded sea ice concentration data (see Appendix). Higher values indicate less severe ice conditions.

4 Methods

As shown in Figure 3, Arctic sea ice extents have generally been decreasing over the post-1953 period of this study. The Beaufort Sea is a prime example of a region in which summer and autumn sea ice coverage has been decreasing, although winter (March) sea ice extent in the Beaufort Sea shows no trend or variability because the ice edge extends to the coastline in March of every year, essentially eliminating year-to-year variations. Consistent with the September decrease of Beaufort ice extent, the BSI has been increasing over the past few decades (Figure 2). Two time series containing trends over time can show a correlation simply because the trends are present in the time series. A trend can be used as a predictive tool by assuming its continuation into the future. However, a trend can inflate persistence-based forecast skill when a variable is used to predict itself (assuming the historical trend continues into the future). Indeed, depictions of time-variations of a quantity such as sea ice extent are often shown as departures from a trend line in order to highlight the interannual variations. One of our main interests in this study is whether or not interannual variations of preceding regional ice extents correlate with later BSI values. In order to exclude the effect of the overall trends in the correlation of these time series, we detrend the data and explore various methods for doing so.

The choice of a function with which to de-trend the time series should be determined by features of the series itself. The detrended time series should exclude the general tendency to change over time, but preserve a measure of the year-to-year variability of the series. The previous studies cited in Section 2 (e.g., Blanchard-Wrigglesworth et al., 2011; Sigmund et al., 2013; Day et al., 2014; Bushuk et al., 2017, 2017) have generally relied on least-squares linear fits for detrending. Goldstein et al. (2016, 2018), by contrast, showed that discontinuous changes in the mean better captured time series (such as open water area) characterized by abrupt changes. In the spirit of the Goldstein et al. studies, we explore various options for detrending a time series such as those in Figures 2 and 3, for which the changes are more pronounced in

recent decades than in earlier decades. In such cases, a single multi-decadal trend line cannot be expected to optimally represent the historical evolution.

We explored several functional forms which fit the time series, including linear, quadratic, cubic, and exponential functions. We found that a simple two-piece linear function – wherein the data are modeled by two line segments that intersect at a 'break-point' year – had the lowest average RMS difference between the time series and the fitted function, although fits using other functions had only slightly larger RMS differences. This choice of the detrending fit has the additional feature of giving a sense of when the ice extent began to change more rapidly.

The two-piece linear fits were obtained by using standard statistical algorithms. A function defined by two intersecting half-lines can be specified by the coordinates of one point on each half-line and the intersection point. With the x-axis as time, and the y-axis as the value of the sea ice extent, the x-values of the non-intersecting points can be chosen to be 1953 and 2013, the first and last years of the BSI dataset. This leaves four values for the function to fit: the series value in 1953, the series value in 2013, and the year and value at the intersection point, also referred to here as the break-point. We note that the break-point is not specified by the user but is determined by the algorithm so that the fit to the time series is optimized. The "curve_fit" function is defined in lines 504-794 of the file https://github.com/scipy/scipy/blob/master/scipy/optimize/minpack.py This function performs a least-squares fit to the function by modifying the function's parameters. A starting "guess" of the function parameters is provided by the user. The linear algebra methods of the *scipy* numerical library is then used.

The two-piece linear fit was generated by allowing the SciPy 'curve_fit' routine (Jones et al., 2001) to iterate to a solution. The "curve_fit" function is defined in lines 504-794 of the minpack.py routine (https://github.com/scipy/scipy/blob/master/scipy/optimize/minpack.py, accessed 27 Dec 18). This function performs a least-squares fit to the function by modifying the function's parameters. A starting "guess" of the function parameters is provided by the user. The linear algebra methods of the scipy numerical library are then used to detrend the BSI values as well as the time series of the regional and pan-Arctic ice extents. In Figure 4, we show the piecewise linear fit together with quadratic, cubic and exponential fits to the time series of the BSI and the September Beaufort Sea ice extent. In the case of the two-piece linear fit, the break-point (chosen to minimize the departures from trend) is in the early 1990s for both sea ice

metrics. It is visually apparent from Figure 4 that all four fits are comparable in terms of the overall magnitudes of the departures from the trend lines. The root-mean-square departures from the various trend lines indeed differed by less than 10%. Given the small differences between the fits, we choose the two-piece linear for the remainder of this study. Because the break-points are computed separately for each region, the use of the two-piece linear fit allows comparisons of the timing of the break-points across the various subregiona.

After using the 'linregress' method from the SciPy (Jones et al., 2001) software library to fit a line to regional monthly extent values and the BSI, we computed correlations between the departures of the two time series from their respective two-piece trend lines. For comparison, we also computed correlations between the "raw" (with trends) time series. The square of the Pearson correlation coefficient (R^2) was computed using the 'stats' method from the SciPy package and was used to determine whether and how strongly the two time-series are correlated with each other.

5 Results

As noted in Section 2, previous studies (e.g., Bushuk et al., 2018) have evaluated the persistence of regional ice extent over the post-1978 period of satellite observations. Here we extend this evaluation to encompass a longer period dating back to 1953 in order to assess the stability of the persistence statistics. Specifically, for each region in Figure 1, we have correlated the September ice extent with the ice extent of antecedent months for the 1953-2013 and 1979-2013 periods. Figure 5 compares these persistence values (autocorrelations at multimonth lags), for the antecedent months of March, May and July in a subset of regions. Because the regions chosen were those that have interannually varying ice cover in September, regions such as the Bering Sea, Hudson Bay, the Sea of Okhotsk and the Baltic Sea were excluded. The correlations were computed before and after a detrending of the data, although only the results for the non-detrended data are shown in Figure 5. For most of the regions, the inclusion of the earlier decades does not have a notable impact on the persistence from July to September. However, the March-to-September and May-to-September correlations change substantially in a few regions. The Baffin Bay March-to-September correlations increase from 0.00 to 0.34 when the earlier decades are eliminated, largely as a result of the post-1979 trend: the post-1979 correlation is statistically significant ($p < 0.05$), while the corresponding correlation based on detrended data is

not significant. The pan-Arctic correlations for all three antecedent months also increase when the earlier decades are eliminated. In the Greenland Sea, the correlations from March and May decrease substantially and lose statistical significance when the earlier decades are eliminated. In this case the March-to-September and May-to-September correlations are again reduced to insignificance by detrending. Although the results for the detrended data are not shown graphically, the detrending generally reduces the significance of the correlations between September and the earlier months, both for the longer post-1953 periods and the shorter post-1979 periods: The March-to-September correlations based on the detrended data for the longer/shorter periods are: -0.05/0.20 for Baffin Bay, 0.20/0.13 for the Barents Sea, 0.00/0.00 for the Beaufort Sea (no March variance), 0..00/0/00 for the Canadian Archipelago (no March variance), -0.15/0.00 for the Chukchi Sea, 0.07/0.21 for the East Siberian Sea, 0.25/-0.03 for the Greenland Sea, 0.03/0.03 for the Kara Sea, and 0.07/0.18 for the Laptev Sea. The corresponding 5% significant levels are 0.26/0.33. Evidently, the springtime "predictability barrier" (Lindsay et al., 2008; Day et al., 2014; Bushuk et al., 2018) in regional forecasts based on persistence of ice extent anomalies is not reduced by the inclusion of several decades of pre-satellite data.

Because changes of trend have not been addressed systematically in previous evaluations of Arctic sea ice trends, we synthesized the break-point information across all regions and calendar months (January-September) included in our study. The synthesis was limited to only those regions and calendar months in which the two-piece linear fit reduced the root-mean-square residual by at least 5% relative to the one-piece linear best fit. Figure 6 groups the break-points into five year periods ending in 1955, 1960,…, 2015. In order to capture the seasonality of the break-points, we present separate plots for (a) the entire January-September period, (b) January-March (winter), (c) April-June (spring), and July-September (summer). As shown in panel ((a), nearly all the break-points occur in the second half of the study period, with a maximum in 1991-1995. The 1991-1995 period has the most break points of any 5-year period, and the 1990s have nearly as many break points as all the other decades combined. The winter and summer seasons are the primary contributors to the maximum in the 1990s, as the spring break points are evenly distributed through the latter half of the study period. However, spring has the fewest (12) break-points overall, while the summer has the most (26). The break-points for our focal metrics, the BSI and September pan-Arctic ice extent, are 1991 and 1996, respectively, consistent with the distribution in Figure 6. These two metrics are included in the results summarized in Figure

6. One may conclude that the 1990s, and to a lesser early 2000s, represent the shift to a more rapid rate of sea ice loss. If one is to argue for a "regime shift" in Arctic sea ice loss (Lenton, 2012), this period would be the leading candidate.

In order to illustrate the effect of the detrending and to show which regions contribute the most explained variance to pan-Arctic sea ice extent, Figure 7 shows the squares of the correlations (R^2) between September pan-Arctic ice extent and the concurrent ice extent in each of the subregions. The R^2 metric is used rather than R because R^2 corresponds to the explained variance. The figure shows values of R^2 before detrending (upper numbers, regular font) and after detrending (lower numbers, bold font). With the trend included, the R^2 values are relatively high in most regions (except for the Bering Sea), ranging from 0.32 to 0.71; the corresponding correlations (R) range from 0.57 to 0.84. These correlations all exceed the 95% significance thresholds, which range from 0.26 ($R^2 = 0.07$) for a 60-year sample with no autocorrelation to 0.38 ($R^2 = 0.14$) for a 60-year sample with an autocorrelation of 0.4. None of the regional or pan-Arctic ice extent autocorrelations exceeded 0.40. Because these correlations are dominated by the trend, the larger values appear in the regions with trends that are most similar to the pan-Arctic trend. When the data are detrended, the correlations are much smaller (R^2 values in bold font in Figure 7) although still larger than the 95% significance thresholds for a 60-year sample ($R = 0.26$, $R^2 = 0.07$). These smaller values indicate the relative contributions of regional variations to the interannual variations of pan-Arctic ice extent. According to Figure 7, the regions contributing most strongly to September pan-Arctic sea ice variations (including trends) are the Beaufort, Chukchi and East Siberian Seas. After the data are detrended, the regions contributing most to September pan-Arctic sea ice variations are the East Siberian and Laptev Seas. The somewhat surprisingly large contribution of the Laptev Sea is consistent with the "dynamical preconditioning" hypothesis of Williams et al. (2016). The variances of the detrended September extents of East Siberian and Laptev Seas are indeed among the largest of all the regions, although the Chukchi Sea's interannual variance is essentially as large.

Figure 8 shows the squares of the correlations between the annual BSI and regional September ice extent before the detrending of both variables (top numbers) and after detrending (bottom numbers). While the actual correlations between the BSI and regional extent are generally negative, the R^2 values plotted in Figure 8 are positive. Large values of R^2 appear in most regions when the trend is included (upper numbers) because the BSI has a strong positive

394 trend over time while September ice extent in most regions has a negative trend. The R^2 values
395 are much weaker in regions away from the Beaufort Sea when the trends are removed (lower
396 numbers in Fig. 8). The detrended R^2 values show the spatial representativeness of the BSI as a
397 measure of interannual variations. Figure 8 shows that the regions of significant explained
398 variance include the Canadian Archipelago to the east as well as the Chukchi Sea to the west.
399 However, the "scale of influence", if measured by the area of significant correlation, is smaller
400 for the BSI in Fig. 8 than for pan-Arctic ice extent in Fig. 7.
401 Because the potential for seasonal predictions is a key motivation for this study, we
402 examine cross-correlations in which the predictands (pan-Arctic ice extent and the BSI) lag
403 potential predictors (regional ice extents) by intervals ranging from zero (no lag) to several
404 seasons. Cross-correlations between non-detrended and detrended September pan-Arctic and
405 regional ice extents are summarized in Tables 1 and 2 respectively. Cross-correlations between
406 non-detrended and detrended BSI and regional ice extent are given in Tables S1 and S2
407 respectively. In all cases, the numerical values are the R^2 values. In order to illustrate the
408 contribution of the trend to the apparent forecast skill, we present these correlations graphically
409 for the regions which show the strongest associations with the September predictands. Figure 9
410 shows the R^2 values for cases in which September pan-Arctic ice extent lags by 0, 1, 2,…,8
411 months the ice extent in four subregions: the Beaufort, Chukchi, East Siberian and Barents Seas.
412 The red bars correspond to correlations computed from the data with the trends included. Not
413 surprisingly, the R^2 values are largest at zero lag. The rates at which the correlations decrease
414 with increasing lag vary regionally, reaching zero by 3-4 months for the Beaufort, Chukchi, and
415 East Siberian Seas. The zero-month lag values are quite large for the Beaufort, Chukchi, and East
416 Siberian regions, where they exceed $R^2 = 0.7$ ($R = 0.84$).
417 However, after detrending (using the two-piece linear best fits), most of the apparent forecast
418 skill is lost. As shown by the blue bars in Figure 9, nearly all the predictability from the Barents
419 and Chukchi Seas vanishes with the detrending, while only small fractions of explained variance
420 remain at non-zero lags when sea ice extents for the Beaufort and East Siberian Seas are the
421 predictors. For example, when the regional extent leads by two months (July), the fractions of
422 explained variance are approximately 0.16 and 0.10 ($R \sim 0.40$ and 0.32) for the East Siberian and
423 Beaufort Seas, respectively. The implication is that the persistence of interannual variations about
424 the trend line makes only small contributions to interannual variations of pan-Arctic sea ice extent,

and that these small contributions result mainly from the Pacific sector of the Arctic. As indicated by Figure 9, the pan-Arctic extent of July and August correlates more highly than any regional extent with September pan-Arctic ice extent in both the non-detrended and the detrended data (see also Tables 1 and 2). The finding that the lagged pan-Arctic correlations exceed the lagged regional vs. pan-Arctic correlations is consistent with the perfect-model results in Bushuk et al.'s (2017) Figure 2, although this comparison is not apples-vs.-apples: Bushuk et al. show the skill of predictions of regional extent (not pan-Arctic extent) in their regional panels. The same is true for Day et al.'s (2014) Fig. 11 and for Bushuk et al.'s (2018) Figs. 6, 9, 10 and 11.

The lagged R^2 values relevant to predictions of the Barnett Severity Index are shown in Figure 10. Because the BSI is based primarily on ice conditions in the Beaufort Sea in August and September, it is not surprising that the correlation is largest for the Beaufort's ice extent in September, when the R^2 value is approximately 0.8 for data that are not detrended. The August and September values for the Chukchi are essentially as large as the corresponding Beaufort values, indicating a spatial coherence of the variations (with trends included) in the two regions. The antecedent extents in the East Siberian and Barents regions also explain significant fractions of the variance when the trends are included.

The blue bars in Figure 10 are the lagged R^2 values based on the detrended data. Because the trend's contribution to the forecast skill has been removed, these correlations provide the most meaningful assessment of the seasonal forecast skill if the BSI based on antecedent ice conditions. The largest correlations are for the Beaufort Sea, where the explained variances decrease from about 0.55 ($R \sim 0.74$) in September to about 0.10 ($R \sim 0.32$) in June. The correlations for the Chukchi are only slightly smaller, but the BSI variance explained by all other regions is less than 10%. The percentage of explained variance is less than one might have anticipated, given that the BSI includes information on the length of the navigation season, which can begin well before September, i.e., as early as July in some years.

6 Conclusion

The substantial decrease of Arctic sea ice over the past several decades is well documented (Cavalieri and Parkinson, 2012; Parkinson, 2014; Onarheim et al., 2018). Of all the regions considered here, only the Bering Sea does not show a negative trend (Onarheim et al., 2018, their Table 1), although the extreme minima of Bering Sea ice during the past two winters (2016-17

and 2017-18) are starting to bring the Bering's trend into alignment with the other regions of the Arctic.

The prominence of the trends in the time series of regional as well as pan-Arctic ice extent makes it important to distinguish the contribution of the trend from other sources of forecast skill. In this study we explored the use of several methods of detrending in order to evaluate the use of ice anomaly persistence (autocorrelation) and regional cross-correlations as predictors of ice variations. The two-piece linear trend evaluations generally have break-points in the 1990s, indicating that the rate of ice loss has been greater in the past two decades than in the earlier portion of the satellite era that began in 1979.

Based on the raw (not detrended) time series, the antecedent ice extents in a substantial fraction of the Arctic regional seas provide significant predictive skill for September pan-Arctic ice extent as well as for the Barnett Severity Index, which is more specific to the Beaufort Sea. Significant portions of variance of both September metrics are explained by the regional ice extents of prior seasons. However, this predictive "skill" is attributable primarily to the trends in the data. Removal of the trend leaves little forecast skill beyond a month or two when the forecast method is limited to the relatively simple statistical correlations utilized here. The low skill for the detrended September pan-Arctic ice extent is consistent with the findings of Stroeve et al. (2014) based on the Sea Ice Outlook as part of the Study of Environmental Arctic Change (SEARCH). Moreover, our inclusion of data back to the early 1950s shows that springtime "predictability barrier" in regional forecasts based on persistence of ice extent anomalies is not reduced by the inclusion of several decades of pre-satellite data.

It must be noted that other sea ice prediction approaches have outperformed persistence (e.g., Tivy et al.,2007; Shröder et al., 2014; Yuan et al., 2016; Petty et al., 2017; and Bushuk et al., 2018). These studies have either used other predictors or made use of the perfect model approach. With regard to the latter, persistence-derived predictability is greater in perfect models than in corresponding operational forecasts, as even some of the perfect-model studies show (Blanchard-Wrigglesworth et al., 2011; Bushuk et al., 2018). With regard to the former, the SIPN is the acid test of the current state of sea ice prediction (at least for September pan-Arctic ice extent) because many contributions utilized predictors other than persistence. A compilation of SIPN results from 2008-2018 shows that, on balance, the SIPN consensus forecasts outperform detrended anomaly persistence by only a small amount. (In this case, persistence was evaluated

from the yearly September mean ice extents in the National Snow and Ice Data Center's G02135_v3.0: ftp://sidads.colorado.edu/DATASETS/NOAA/G02135/seaice_analysis/, accessed 27 Dec 2018). The mean absolute error of the median SIPN forecasts issued in July of 2008-2018 is 0.32 million km^2, while the error of a forecast of persistence of the previous September's deviation from the trend line is 0.37 million km^2. Simple persistence of the previous year's actual value has an error of 0.40 million km^2. The corresponding root-mean-square errors are 0.57, 0.68 and 0.67 million km^2. While those persistence metrics are based on year-to-year September variations, the SIPN forecasts for September are made in June, July and August -- less than a season prior to September, and on the favorable side of the springtime "prediction barrier". At least in this particular application, which represents the state of the art in seasonal sea ice forecasting, sea ice anomaly persistence is a challenging control forecast and may even be regarded as a respectable competitor.

While there is statistical significance in the trend-derived skill at lead times of several seasons and also in the remaining (detrended) skill at lead times of a month or two, statistical significance does not equate to usefulness. Potential users of sea ice forecasts include local communities engaging in offshore subsistence and travel activities, marine transport companies, offshore resource extraction, and the tourism industry. The relatively small fractions of variance predictable several months in advance using detrended data (Figures 6-9) will likely leave uncertainties that are too great for many users. However the trend-derived skill, which can represent 50% or more of the variance, may enable decisions if the interannual variations superimposed on the trend represent acceptable risks for users of sea ice forecasts.

Acknowledgments

Funding for this work was provided by the Climate Program Office of the National Oceanic and Atmospheric Administration through Grants NA16OAR4310162 and by the National Science Foundation through Grant OPP-1749081. Florence Fetterer was supported by the CIRES/NOAA Cooperative Agreement, NOAA Grant NA15OAR4320137. We thank the two reviewers for their helpful comments.

References

Agnew, T. A., and Howell, S.: Comparison of digitized Canadian ice charts and passive microwave sea-ice concentrations. Geoscience and Remote Sensing Symposium, 2002. IGARSS '02. 2002 IEEE International 1: 231- 233. doi: 10.1109/IGARSS.2002.1024996, 2002.

AMAP: Snow, Water, Ice and Permafrost in the Arctic: 2017 Update. Arctic Monitoring and Assessment Programme, Oslo, Norway, xiv + 269 pp., 2017.

Barnett, D. G.: A long-range ice forecasting method for the north coast of Alaska. Sea Ice Processes and Models, R. Pritchard, Ed., University of Washington Press, 402–409, 1980.

Blanchard-Wrigglesworth, E., Armour, K. C., and Bitz, C. M.: Persistence and inherent predictability of Arctic sea ice in a GCM ensemble and observations. J. Climate, 24, 231-250, 2011.

Box, J. E., and 19 Coauthors: Key indicators of Arctic climate change, 1971-2017. Environmental Research Letters, in press.

Bushuk, M., Msadek, R., Winton, M., Vecchi, G. A., Gudgel, R., Rosati, A., and Yang, X.: Skillful regional predictions of Arctic sea ice on seasonal timescales. Geophysical Research Letters, 44, 4953-4964, doi:10.1002/2017/GL073155, 2017.

Bushuk, M., Msadek, R., Winton, M., Vecchi, G., Yang, X., Rosati, A., and Gudgel, R.: Regional Arctic sea-ice prediction: potential versus operational seasonal forecast skill. Climate Dynamics, https://doi.org/10.1007/s00382-018-4288-y, 2018.

Cavalieri, D. J., and Parkinson, C. L.: Arctic sea ice variability and trends, 1979-2010. Cryosphere, 6, 881-889, 2012.

Crowley Maritime Corporation, 2002. From http://www.crowley.com/content/download/11926/80932/version/1/file/Alaska-50-Years.pdf accessed 10 May 2018.

Day, J. J., Tietsche, S., and Hawkins, E.: Pan-Arctic and regional sea ice predictability: Initialization month dependence. J. Climate, 27, 4371-4390, 2014.

Drobot, S.: Long-range statistical forecasting of ice severity in the Baaufort-Chukchi Sea. Weather and Forecasting, 18, 1161-1176, 2003.

Drobot, S. D., J. A. Maslanik, and Fowler, C. F.: A long-range forecast of Arctic summer sea0ice minimum extent. Geophysical Research Letters, 33, L10501, doi:10.1029/2006/GL026216, 2006.

Goldstein, M. A., Lynch, A. H., Arbetter, T. E., and Fetterer, F.: Abrupt transitions in Arctic open water area. The Cryosphere Discussion, doi:10.5194/tc-2016-108, 2016.

Goldstein, M. A., Lynch, A. H., Zsom, A., Arbetter, T., Chang, A., and Fetterer, F.: The step-like evolution of Arctic open water. Nature Scientific Reports, 8:16902, doi:10.1038/s41598-018-35064-5, 2018.

Guemas, V., and 12 Coauthors: A review on Arctic sea-ice predictability and prediction on seasonal to decadal time-scales. Quarterly J. Royal Meteor. Soc., 142, 546-561, 2016.

Holland, M. M., Bailey, D. A., and Vavrus, S.: Inherent sea ice predictability in the rapidly changing Arctic environment of the Community Climate System Model, version 3. Climate Dynamics, 36, 1239-1253, 2011.

Jones E., Oliphant, E. Peterson E. *et al.:* SciPy: Open Source Scientific Tools for Python, 2001-, http://www.scipy.org/ [Online; accessed 2018-03-29].

Kinnard, C., Zdanowicz, C. M., Fisher, D. A., Isaksson, E., De Vernal, A., and Thompson, L. G.: Reconstructed changes in Arctic sea ice over the past 1,450 years. Nature, 479, 509-512, 2011.

Kwok, R., and Rothrock, D. A.: Decline in Arctic sea ice thickness from submarine and ICESat records: 1958-2008. Geophys. Res. Lett., 36, L15501, 2009.

Laxon, S.W., Giles, K. A.. Rideout, A. L., Wingham, D. J., Willatt, R., Cullen, R., Kwok, R., Schweiger, A., Zhang, J.,. Haas, C., Hendricks, S., Krishfield, R., Kurtz, N., Farrell, S., and

565 Davidson, M.: CryoSat-2 estimates of Arctic sea ice thickness and volume. Geophys. Res.
566 Lett., *40*, doi: 10.1002/grl.50193, 2013.

567 Lenton, T. M.: Arctic climate tipping points. Ambio, 41, 10-22, 2012.

568 Lindsay, R. W., Zhang, J., Schweiger, A. J., and Steele, M. A.: Seasonal predictions of ice extent
569 in the Arctic Ocean. Journal of Geophysical Research (Oceans), 113, C02023,
570 https://doi.org/10.1029/2007/C004259, 2008.

571 Maslanik, J., Stroeve, J., Fowler, C., and Emery, W: Distribution and trends in Arctic sea ice age
572 through spring 2011. Geophys. Res. Lett., 38**,** L13502, doi:10.10029/2011GL047735, 2011.

573 Meier, W., Fetterer, F., Savoie, M., Mallory, S., Duerr, R., and Stroeve, J: NOAA/NSIDC
574 Climate Data Record of Passive Microwave Sea Ice Concentration, Version 2. Boulder,
575 Colorado USA. NSIDC: National Snow and Ice Data Center.
576 doi:http://dx.doi.org/10.7265/N59P2ZTG. (G02202), 2013.

577 National Ice Center and National Snow and Ice Data Center. Compiled by Fetterer, F., Savoie,
578 M., Helfrich, S., and Clemente-Colón,: *Multisensor Analyzed Sea Ice Extent - Northern*
579 *Hemisphere (MASIE-NH), Version 1*. Boulder, Colorado USA. NSIDC: National Snow and Ice
580 Data Center. doi: https://doi.org/10.7265/N5GT5K3K, (G02186), 2010 (updated daily)

581 NOAA: Arctic Report Card 2017. National Oceanic and Atmospheric Administration,
582 ftp://ftp.oar.noaa.gov/arctic/documents/ArcticReportCard_handout2017.pdf (accessed 27 Dec
583 2018)

584 Onarheim, I. H., Eldevik, T., Smedsrud, L. H., and Stroeve, J. C.: Seasonal and regional
585 manifestations of Arctic sea ice. J. Climate, 31, 4917-4932, doi:10.1175/JCLI-D-17-0427.1,
586 2018.

587 Parkinson, C. L.: Spatially mapped reductions in the length of the Arctic sea ice season.
588 Geophys. Res. Lett., 41, 4316-4322, 2014.

589 Partington, K., Flynn, T., Lamb, D., Bertoia, C., and Dedrick, K.: Late twentieth century
590 Northern Hemisphere sea-ice record from U.S. National Ice Center ice charts. J. Geophys. Res.
591 108(C11): 3343. doi:10.1029/2002JC001623, 2003.

592 Petty, A. A., Schröder, D., Stroeve, J., Markus, T., Miller, J., Kurtz, N., Feltham, D., and Flocco,
593 D: Skillful spring forecasts of September Arctic sea ice extent using passive microwave sea ice
594 observations. Earth's Future, 5, 254-263, 2017.

595 Schröder, D., Feltham, D. L., Flocco, D., and Tsamados, M.: September Arctic sea-ice minimum
596 predicted by spring melt-pond fraction. Nature Clim. Change, 4(5): 353–357, 2014.

597 Schweiger, A. J., Wood, K. R., and Zhang, J.: Arctic sea ice volume variability over 1901-2010:
598 A model-based reconstruction. J. Geophys. Res.-Oceans, in review, 2018.
599

600 Serreze, M. C., and Stroeve, J.: Arctic sea ice trends, variability and implications for seasonal sea
601 ice forecasting. Phil. Trans. Royal Society A, 373, 20140159, 2015.

602 Serreze, M. C., Stroeve, J., Barrett, A. P., and Boisvert, L. N.: Summer atmospheric circulation
603 anomalies over the Arctic Ocean and their influences on September sea ice extent: A cautionary
604 tale. J. Geophys. Res.-Atmospheres, 121(19): 11,463-11,485, doi:10.1002/2016JD025161, 2016.

605 Sigmund, M., Fyfe, J. C., Flato, G. M., Kharin, V. V., and Merryfield, W. J.: Seasonal forecast
606 skill of Arctic sea ice area in a dynamical forecast system. Geophysical Research Letters, 40,
607 529-534, doi:10.1002/grl.50129, 2013.

608 Stroeve, J., Hamilton, L. C., Bitz, C. M., and Blanchard-Wrigglesworth, E.: Predicting September
609 sea ice: Ensemble skill of the SEARCH Sea Ice Outlook, 2008-2013. Geophys. Res. Lett., 41,
610 2411-2418, 2014.

611 Tivy, A., Alt, B., Howell, S. E. L., Wilson, K., and Yackel, J.: Long-range prediction of the
612 shipping season in Hudson Bay: A statistical approach. Weather and Forecasting, 22, 1063-1075,
613 2007.

614 Walsh, J. E., Fetterer, F., Stewart, J. S., and Chapman, W. L.: A database for depicting sea ice
615 variations back to 1850. Geograph. Rev., 107, 89-107, 2016.

616 Walsh, J. E., Chapman, W. L., and Fetterer, F.: Gridded Monthly Sea Ice Extent and
617 Concentration, 1850 Onward, Version 1. Boulder, Colorado USA. NSIDC: National Snow and
618 Ice Data Center. doi: http://dx.doi.org/10.7265/N5833PZ5, (G10010), 2015 (updated 2016).

619 Williams, J., Tremblay, B., Newton, R., and Allard, R.: Dynamic preconditioning of the
620 minimum September sea ice extent. J. Climate, 29, 5879-5891, 2016.

621 Yuan, X., Chen, D., Li, C., and Wang, W.: Arctic sea ice seasonal prediction by a linear markov
622 model. J. Climate, 29, 8151-8173, 2016.

Appendix. Reconstruction of the Barnett Severity Index, 1953-2013

As described in Section 2, the Barnett Severity Index (BSI) is a combination of five metrics of ice coverage in the Beaufort Sea. Drobot et al. (2003) used the BSI through 2000 in their evaluation of predictability based on multilinear regression against various measures of sea ice cover. In order to update the BSI for use in this study, we base a reconstruction on the digital grids of sea ice concentration in the Historical Sea Ice Atlas (HSIA) for Alaska (http://seaiceatlas.snap.uaf.edu/ accessed 27 Dec 2018). As with the regional ice extent calculations using G10010 (Section 3), we use the HSIA because it extends the record 26 years back in time before the start of the satellite passive microwave record. While the sources of the ice concentration data in the HSIA are the same as in G10010, a notable advantage of the HSIA is its weekly temporal resolution (vs. the monthly resolution of G10010). The HSIA also has a spatial resolution of ¼° latitude by ¼° degree longitude. Because of the weekly time resolution, the distance metrics (3)-(5) of the BSI are truncated to the nearest week. Similarly, the distance metrics (1) and (2) are truncated to the nearest 27.8 km (15 n mi). One of the within-month dates of the HSIA grids is the 15th of each month, so no temporal interpolation is necessary for metrics (1) and (2). The reconstructed values of the BSI are listed in Table A1.

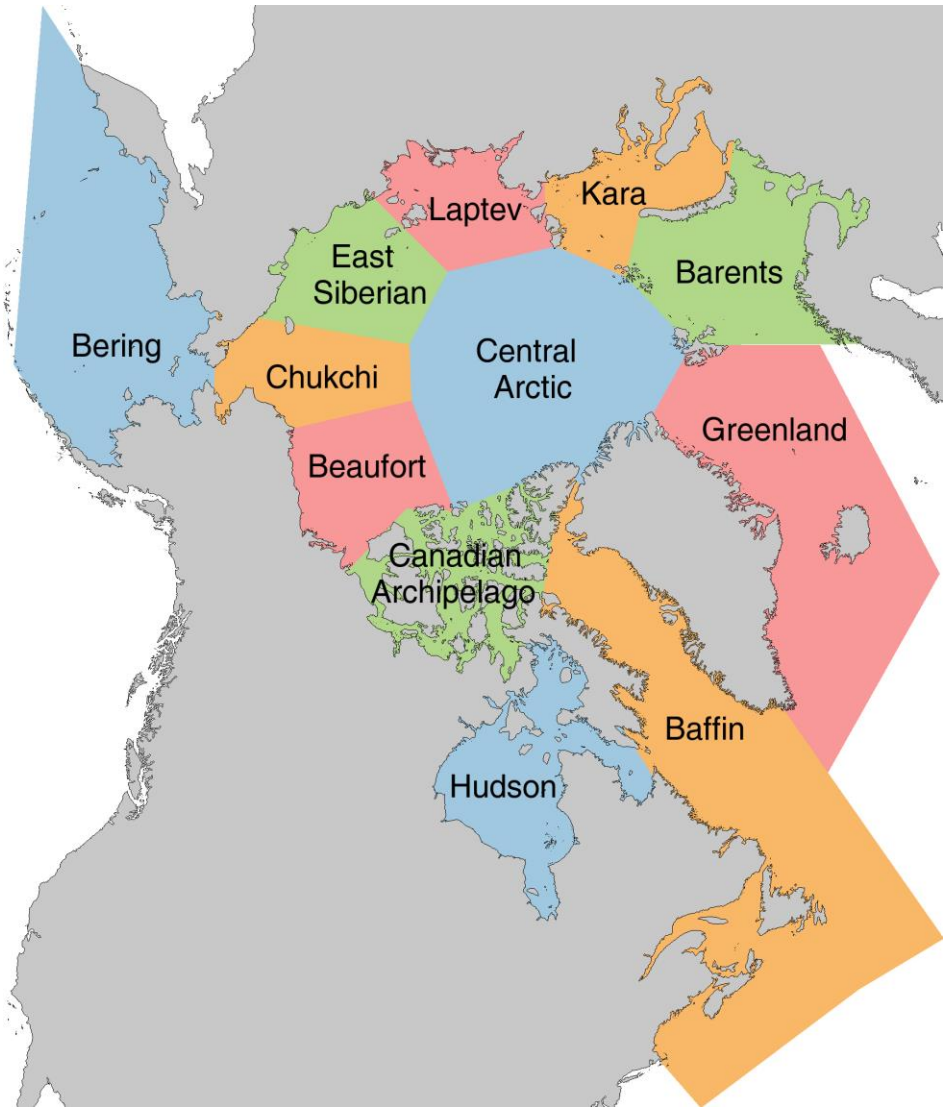

642
643
644 **Figure 1.** The MASIE subregions used in the study (NIC and NSIDC, 2010).
645

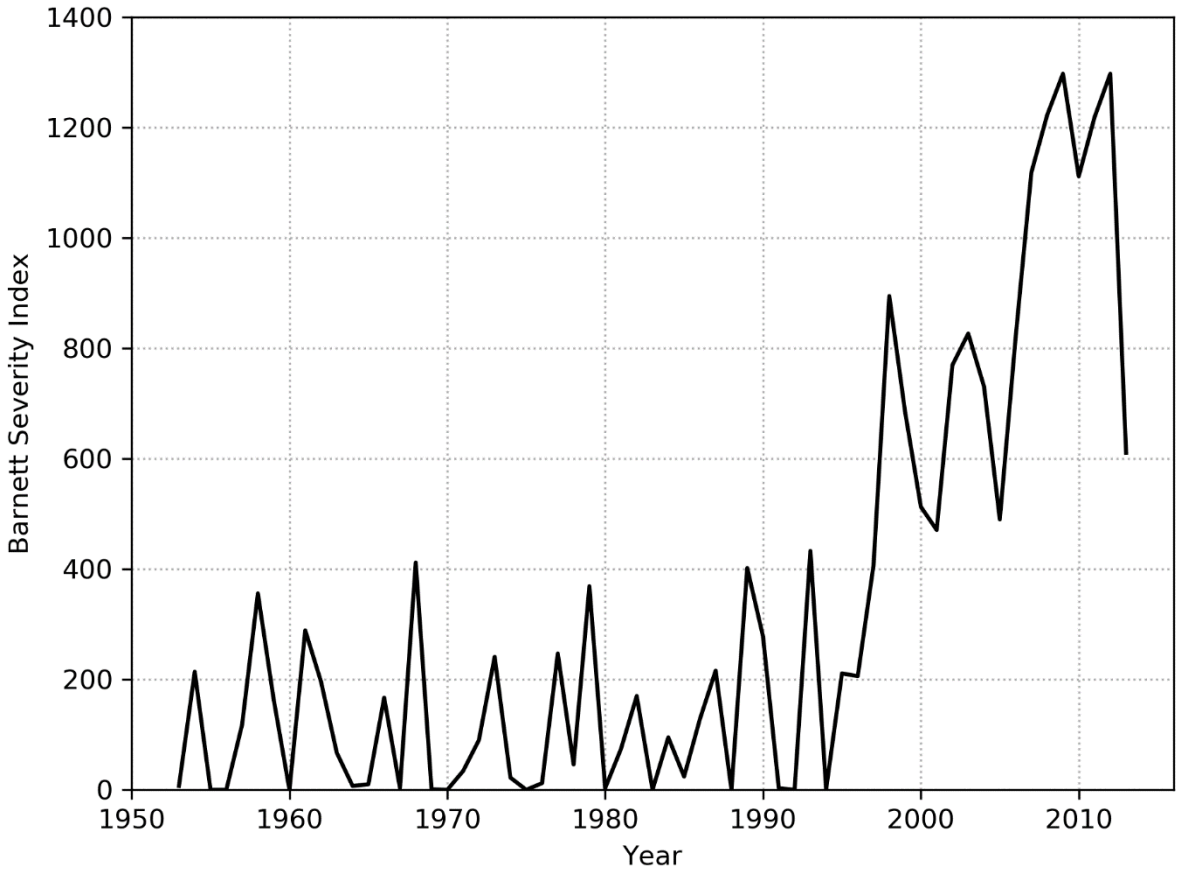

Figure 2. Time series of the Barnett Severity Index (BSI), 1953-2013.

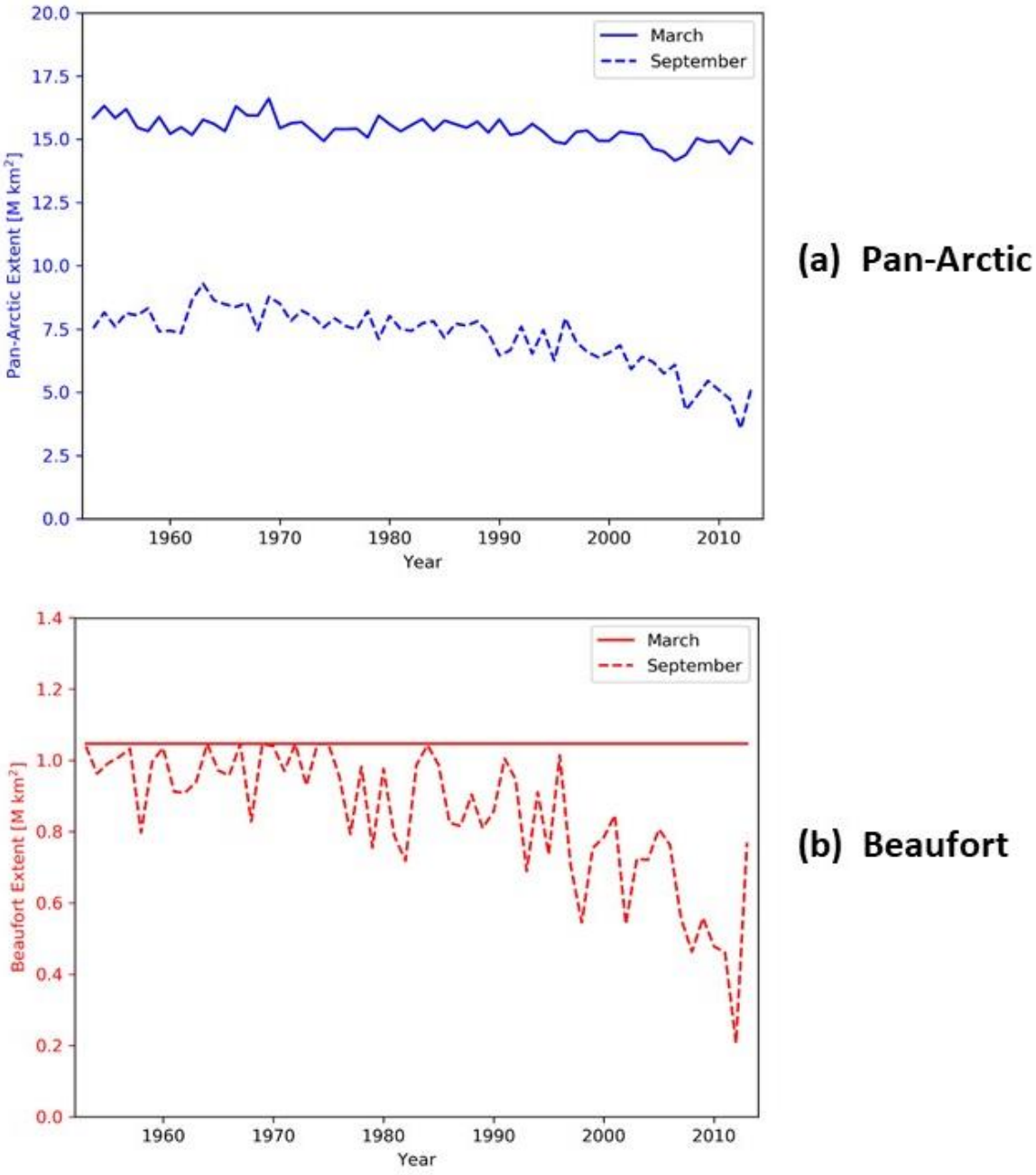

652

653 **Figure 3. (a)** Total Arctic sea ice extent and (b) the extent of ice in the Beaufort Sea during
654 March(solid lines) and September (dashed lines) .

655

656

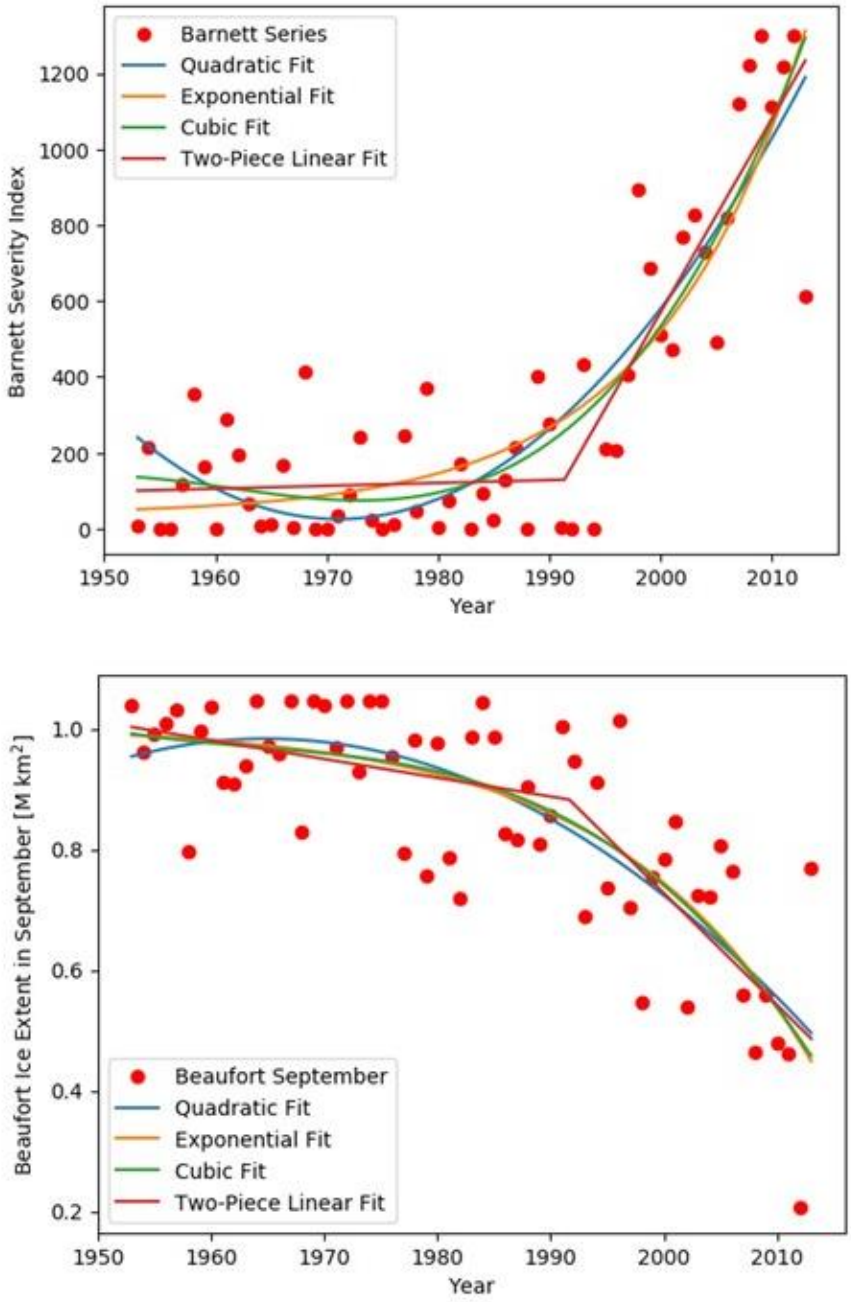

Figure 4. Examples of different fit methods (see legend) applied to the BSI (upper panel) and the September Beaufort ice extent time series (lower panel).

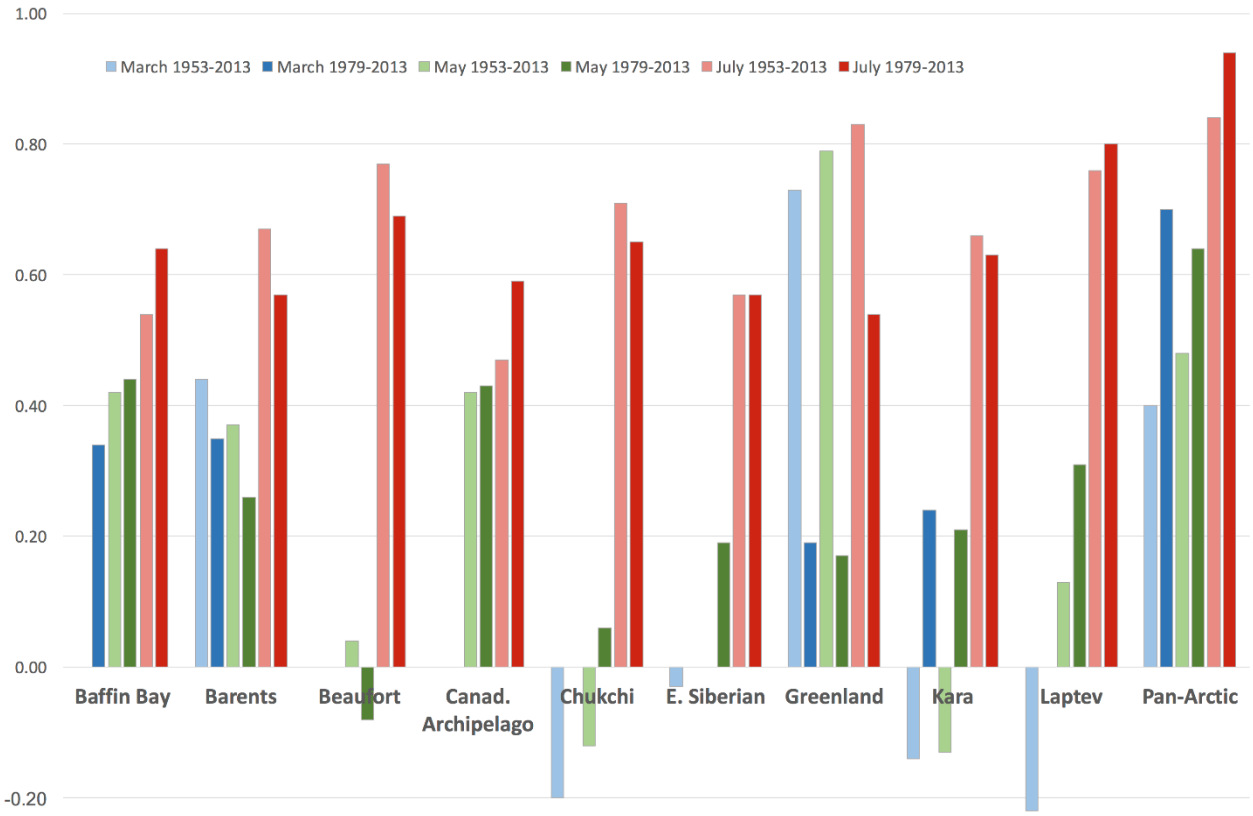

Figure 5. Correlations of September ice extents in individual seas with ice extent in the same region in March (green bars), May (blue bars) and July (red bars). Correlations are also shown for Pan-Arctic extent (far right). The correlations are based on non-detrended data. In each case, light-colored bars are for 1953-2013 and dark-colored bars are for 1979-2013. The absence of a bar indicates a correlation of zero.

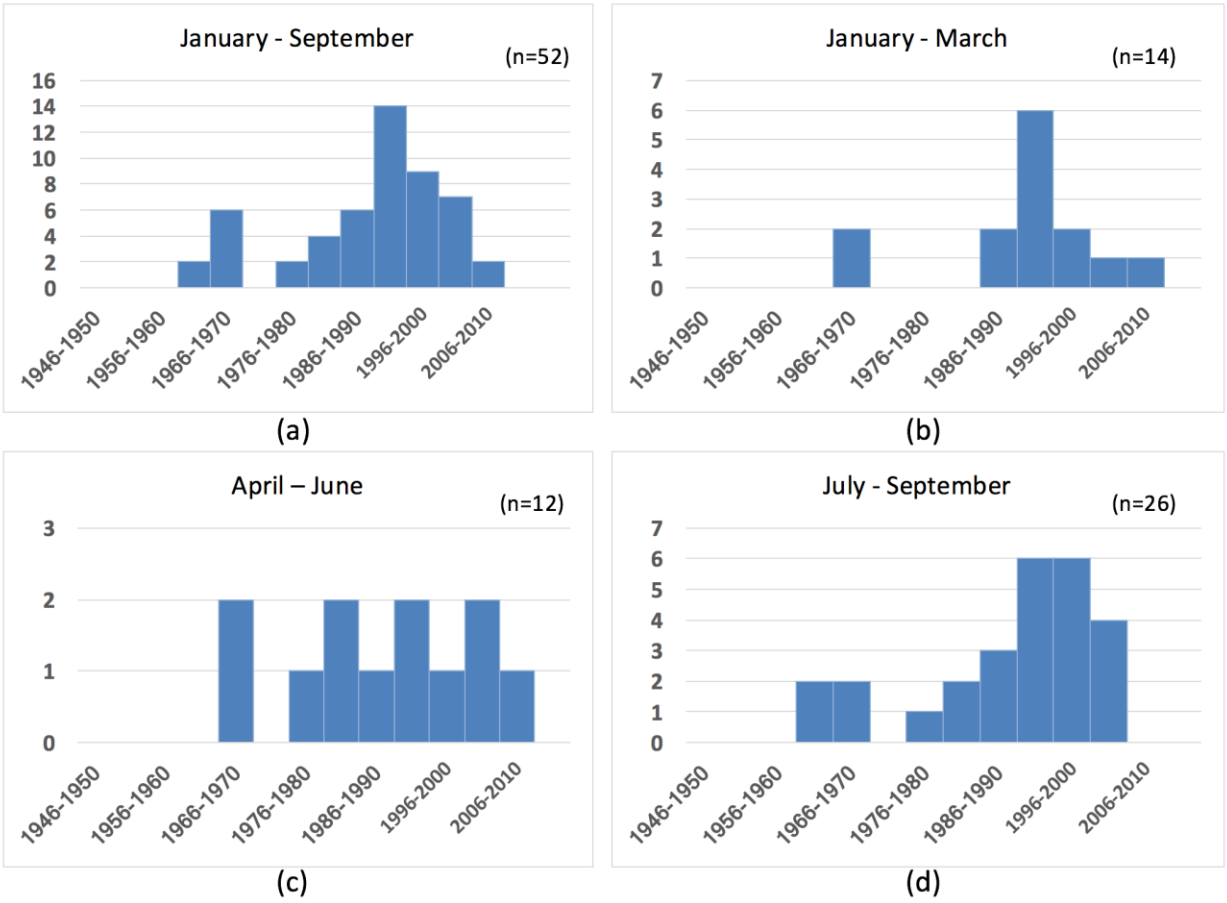

Figure 6. The distribution of break-point years across all regions for (a) January-September and its three subperiods: (b) January-March, (c) April-June, (d) July-September). Only cases for which detrending using two lines, rather than one, reduced the rms error by 5% or more are included. Note that y-axes have different scales.

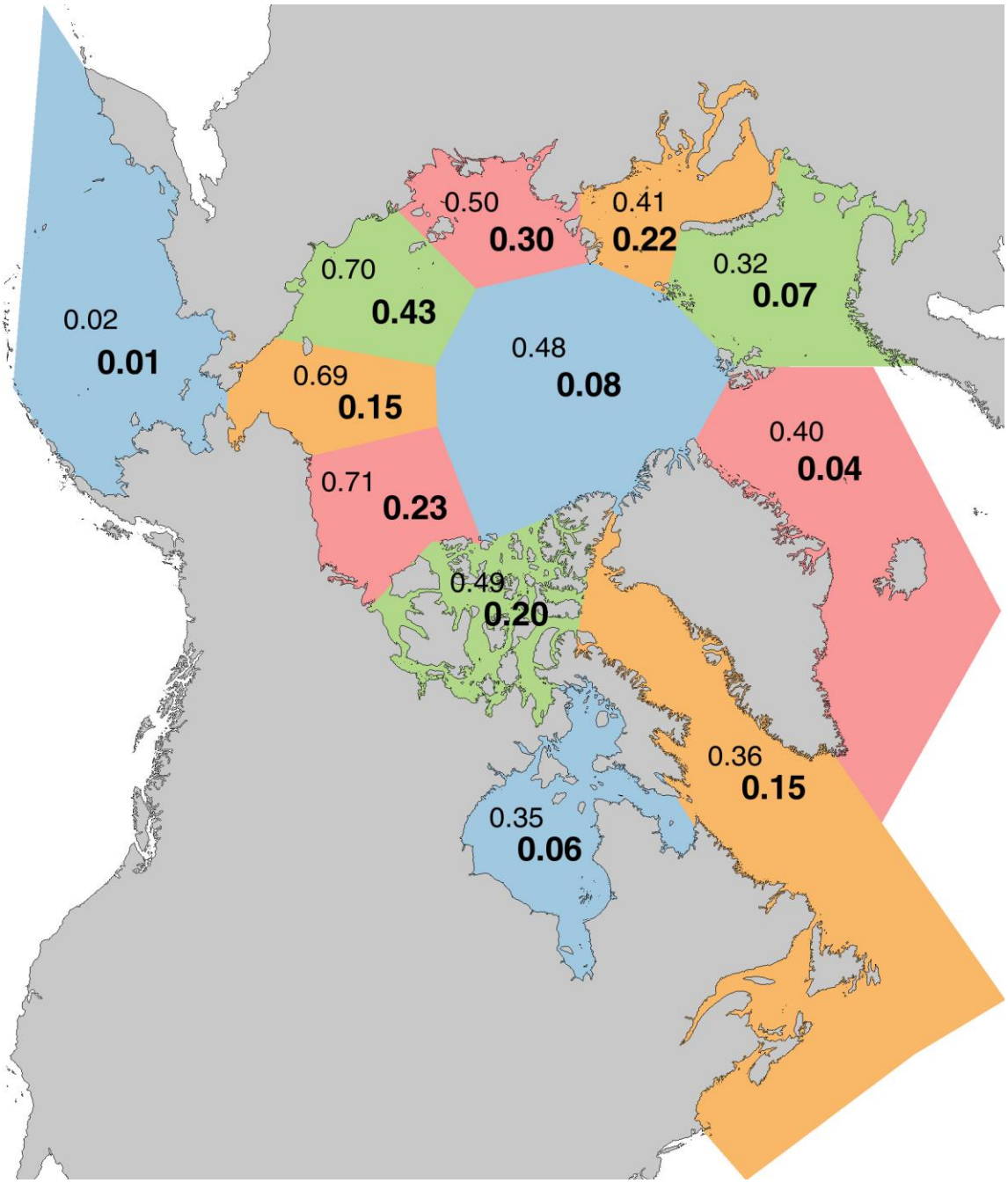

676
677

678 **Figure 7.** Squares of correlations (R^2) between September pan-Arctic ice extent and September
679 regional ice extent based on ice extents including trends (upper numbers in normal
680 font) and detrended (lower numbers, bold font).

681

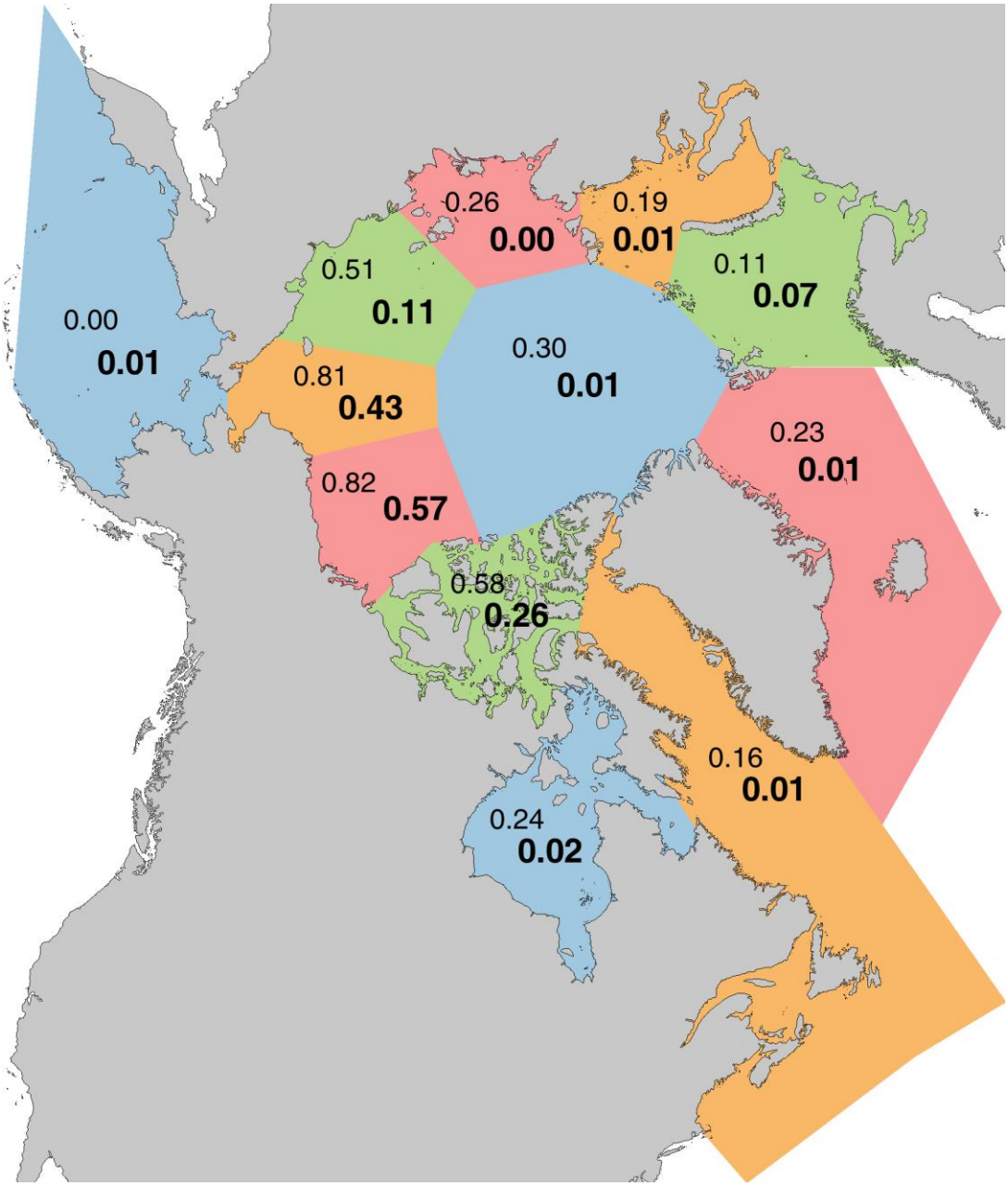

682
683

684 **Figure 8.** As in Figure 7, but for squares of correlations between the annual BSI and September
685 regional ice extents based on raw (not detrended) time series (upper numbers) and
686 detrended time series (lower numbers, bold font).

687

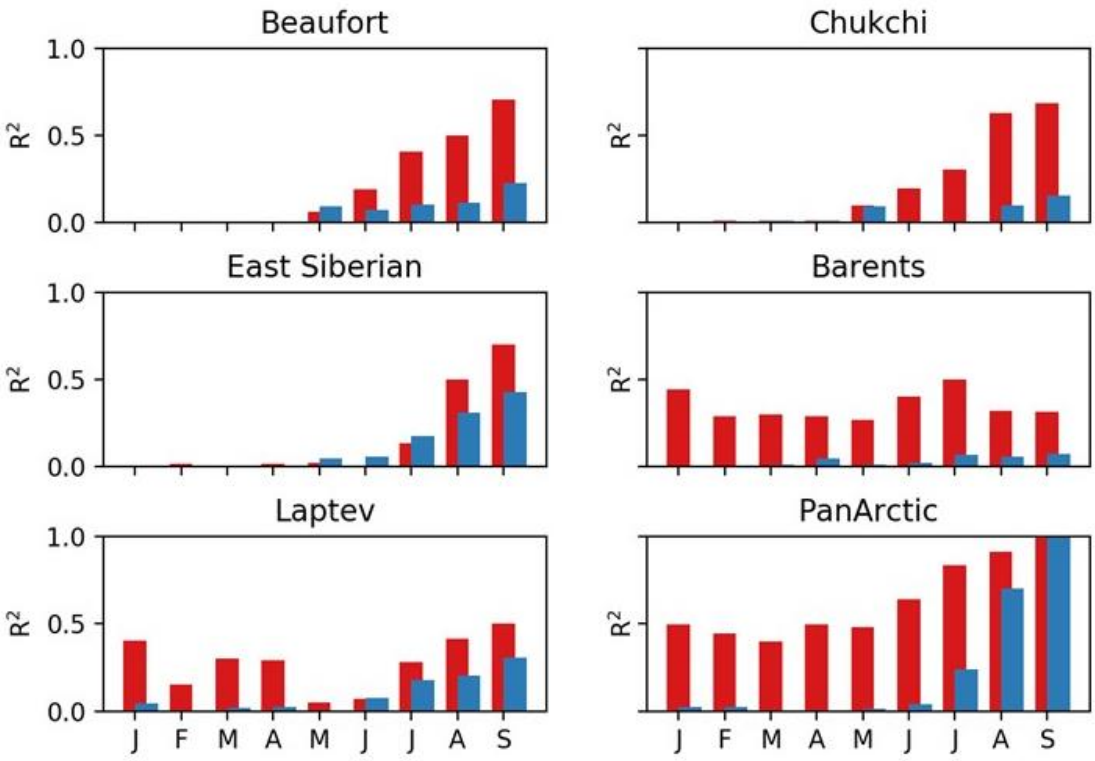

688

689 **Figure 9.** Examples of variances of September pan-Arctic ice extent and explained by correlations
690 with antecedent regional ice extent in individual calendar months from September back
691 to January (pan-Arctic extent lagging by 0, 1, 2, …, 8 months). Correlations are plotted
692 as fractions of explained variance (squares of correlations). Red bars are correlations
693 with trends included, blue bars are correlations after removal of trends.

694

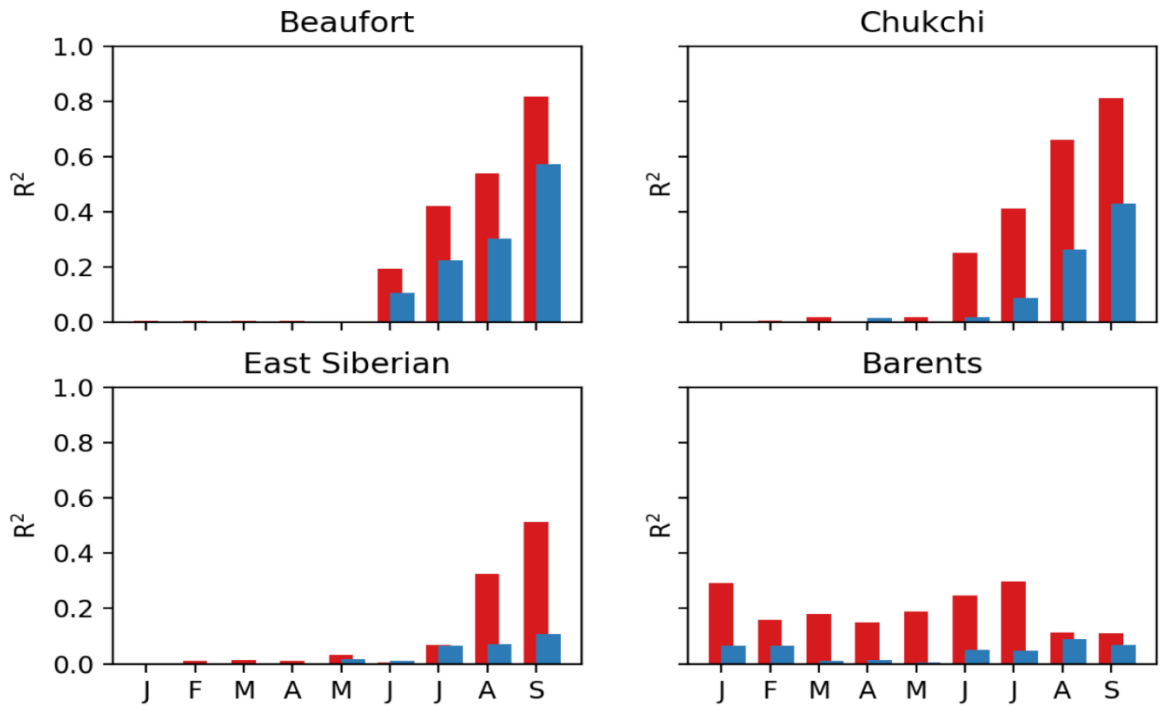

Figure 10. Examples of variances explained by correlations between the Barnett Severity Index and regional ice extent in individual calendar months from September back to January (BSI lagging by 0, 1, 2, …, 8 months). Correlations are plotted as fractions of explained variance (squares of correlations). Red bars are correlations with trends included, blue bars are correlations after removal of trends.

Region	Jan	Feb	Mar	Apr	May	Jun	Jul	Aug	Sep
Baffin-St. Lawrence	0.08	0.06	0.02	0.16	0.32	0.49	0.61	0.52	0.36
Barents	0.45	0.29	0.30	0.29	0.27	0.41	0.50	0.32	0.32
Beaufort	0.41	0.41	0.41	0.41	0.06	0.19	0.41	0.50	0.71
Bering	0.00	0.00	0.01	0.00	0.01	0.12	0.08	0.01	0.02
Canadian Archipelago	0.41	0.41	0.41	0.41	0.00	0.13	0.09	0.52	0.49
Central Arctic	0.21	0.11	0.18	0.01	0.02	0.02	0.15	0.07	0.48
Chukchi	0.00	0.01	0.01	0.01	0.10	0.20	0.31	0.63	0.69
East Siberian	0.00	0.02	0.01	0.02	0.02	0.00	0.14	0.50	0.70
Greenland	0.47	0.53	0.50	0.48	0.43	0.41	0.45	0.29	0.40
Hudson	0.05	0.41	0.41	0.26	0.03	0.32	0.66	0.37	0.35
Kara	0.00	0.03	0.11	0.04	0.10	0.09	0.44	0.42	0.41
Laptev	0.40	0.15	0.30	0.29	0.05	0.07	0.28	0.42	0.50
Pan-Arctic	0.50	0.44	0.40	0.50	0.48	0.64	0.84	0.91	1.00

Table 1. Correlations between monthly regional ice extent and pan-Arctic ice extent expressed as explained variance (R^2). Cases where at least 10% of the variance in pan-Arctic ice extent is explained by regional ice extent in a given antecedent month are highlighted with bolded region names. Levels of shading of boxes denote values exceeding 0.10, 0.20, 0.30,…

Region	Jan	Feb	Mar	Apr	May	Jun	Jul	Aug	Sep
Baffin-St. Lawrence	0.09	0.04	0.08	0.06	0.01	0.00	0.03	0.16	0.15
Barents	0.00	0.01	0.01	0.05	0.01	0.02	0.07	0.06	0.07
Beaufort	0.05	0.05	0.05	0.05	0.10	0.08	0.11	0.11	0.23
Bering	0.01	0.01	0.08	0.03	0.02	0.00	0.01	0.01	0.01
Canadian Archipelago	0.05	0.05	0.05	0.05	0.01	0.02	0.02	0.16	0.20
Central Arctic	0.02	0.02	0.11	0.03	0.02	0.04	0.07	0.00	0.08
Chukchi	0.00	0.00	0.01	0.01	0.10	0.00	0.00	0.10	0.15
East Siberian	0.00	0.00	0.00	0.00	0.05	0.06	0.18	0.31	0.43
Greenland	0.06	0.04	0.09	0.07	0.03	0.06	0.04	0.00	0.04
Hudson	0.00	0.05	0.05	0.01	0.05	0.01	0.11	0.07	0.06
Kara	0.01	0.03	0.03	0.04	0.00	0.18	0.12	0.13	0.22
Laptev	0.05	0.00	0.02	0.02	0.01	0.08	0.18	0.21	0.30
Pan-Arctic	0.03	0.02	0.00	0.00	0.01	0.04	0.24	0.70	1.00

Table 2. Correlations between detrended monthly regional ice extent and detrended September pan-Arctic ice extent expressed as explained variance (R^2). Cases where at least 10% of the variance in September pan-Arctic ice extent is predictable by regional ice extent in a given antecedent month are highlighted with bolded region names. Shading of boxes is as in Table 1.

1953	7	1984	95
1954	213	1985	24
1955	0	1986	178
1956	0	1987	216
1957	117	1988	0
1958	356	1989	402
1959	163	1990	278
1960	0	1991	3
1961	289	1992	0
1962	195	1993	434
1963	66	1994	1
1964	7	1995	211
1965	10	1996	206
1966	167	1997	407
1967	3	1998	895
1968	412	1999	685
1969	1	2000	513
1970	0	2001	471
1971	34	2002	770
1972	90	2003	827
1973	240	2004	731
1974	22	2005	490
1975	0	2006	819
1976	13	2007	1119
1977	247	2008	12239
1978	46	2009	12989
1979	368	2010	1112
1980	3	2011	1219
1981	74	2012	1298
1982	170	2013	611
1983	0		

Table A1. Yearly values of the Barnett Severity Index (BSI). Source: Rebecca Rolph, Geophysical Institute, University of Alaska, Fairbanks.